Time- and Space-Resolved Density Evolution of the Plasma Waveguide

T. R. Clark and H. M. Milchberg

Institute for Physical Science and Technology, University of Maryland, College Park, Maryland 20742

(Received 12 November 1996)

Detailed time- and space-resolved electron density measurements are presented for laser-produced plasma waveguides. A density depression suitable for optical guiding begins to develop within the first few hundred picoseconds after plasma generation, during which rapid cooling occurs. At longer times the expansion closely follows that of a cylindrical blast wave, with further cooling due to expansion work. The waveguide profile is uniform over most of its length, with the density depression appearing within 150 μm of the ends. [S0031-9007(97)02783-X]

PACS numbers: 52.40.Nk, 52.35.Mw, 52.40.Db

The recently developed plasma waveguide has made possible one of the major goals in intense laser-matter interaction physics, that of a large intensity-interaction length product [1]. Applications such as laser-driven electron accelerators [2], generation of high harmonics [3], and soft x-ray laser development [4] would benefit from a large laser-plasma interaction length. Important to all these applications is detailed knowledge of the evolution of the electron density profile forming the waveguide, which determines the propagating mode structure of both the pump laser pulse [5] (which drives the process of interest) and any light generated by it [6], as well as the coupling.

In this Letter, we present detailed measurements of the time and space development of the plasma waveguide electron density, from the onset of laser-driven ionization during the first ~100 picoseconds, to many nanoseconds into the cylindrical blast wave expansion phase. While in previous work we have calculated waveguide formation, and have experimentally demonstrated guiding in the single mode, multimode, and leaky mode regimes, *direct* measurement of the waveguide electron density profile had not been made. The measurements reported here are also of interest as controlled studies of highly nonequilibrium, symmetric plasmas, which can be used as benchmarks for laser-plasma hydrodynamics codes [7].

We note that recent experiments have demonstrated high intensity guiding of laser pulses injected into hollow, evacuated capillaries [8] and high voltage capillary discharges [9], although in this geometry, side viewing of the guiding process or measurement of the refractive index profile has not been possible. In other work, the initial formation and expansion of limited extent ionization channels in gas jet targets has been measured with moiré deflectometry [10]. Channel formation in solid target blowoff plasmas has recently been studied with interferometric methods, where a sufficiently intense pulse of long duration (500 ps) was observed to form a channel through ponderomotive filamentation [11].

The plasma waveguide is generated through the hydrodynamic evolution of a laser breakdown spark generated in the line focus of an axicon lens in a background gas. The initial plasma electrons, produced early in the laser pulse through multiphoton ionization, are heated by the laser pulse via inverse bremsstrahlung absorption, driving further ionization through collisions to a degree determined by the initial gas density. The heated electrons drive the expansion of the plasma into the neutral background gas, resulting in an ion density minimum on axis and a density enhancement (the shock wave) at the periphery from ion-atom and ion-ion collisions. Since the plasma remains essentially charge neutral, the electron density follows the ion density, providing the desired index profile for guiding.

The time- and space-resolved density profiles of this experiment were determined using a folded wave front interferometer in a pump-probe configuration. The pump pulse (1.064 μm, 100 ps pulsewidth, maximum energy 500 mJ) from a Nd:YAG regenerative/power amplifier system [12] generated the plasma waveguide at the ~1 cm long focus of a 35° base angle axicon, at intensities of up to 5×10^{13} W/cm^2. A synchronous probe pulse, split off earlier from the amplifier chain and frequency doubled (~100 μJ at 532 nm and 70 ps width), was passed through a corner cube mounted on an optical delay line with delay relative to the pump of -1 to 11 ns. The 1 cm diameter probe beam was directed transversely through the plasma waveguide, then through a matched two lens system [13] followed by an uncoated BK7 glass wedge plate, producing two vertically separated complementary interferograms. One of these was relay imaged by a 10× microscope objective onto a charge coupled device (CCD) camera and digitized by a frame grabber. The overall system magnification was 23× with resulting spatial resolution of 1.5 μm/pixel. The temporal resolution was set at 70 ps by the probe pulse duration.

The interferograms are two dimensional projected images of the plasma-induced phase shift. A sample interferogram is shown in Fig. 1(a) for the center 300 μm region of a ~1 cm long waveguide generated in a 230/20 torr gas mixture of Ar/N_2O for a delay of 5 ns. The high degree of axial and radial symmetry is evident, and this plays an important role in the data analysis as described below. The top and bottom regions of the image are the wedge fringe pattern from undisturbed portions of the probe beam outside the waveguide. It is important that consideration

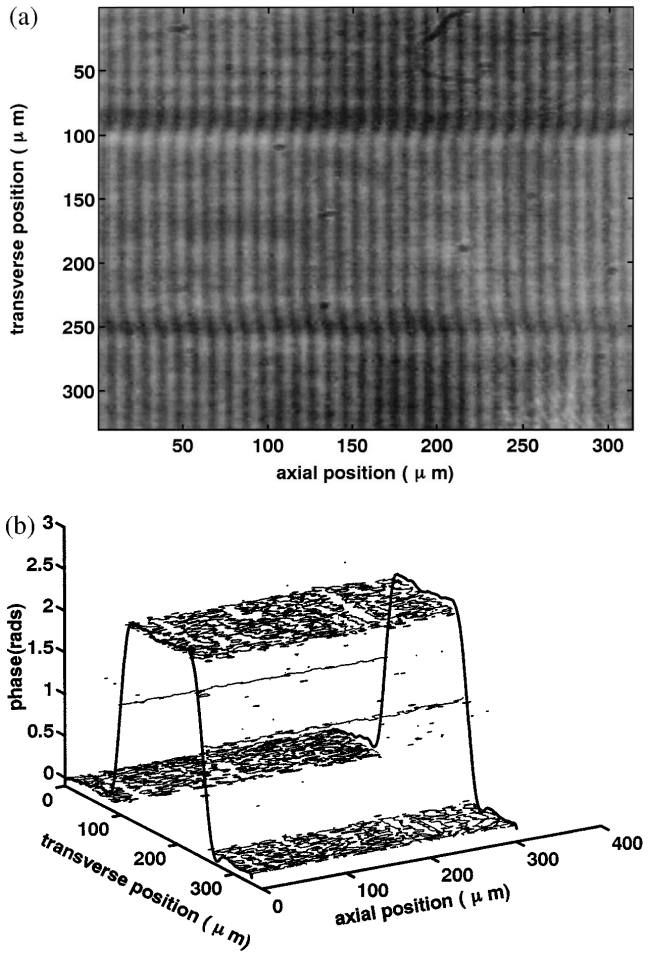

FIG. 1. (a) Interferogram of central 300 μm of a $\sim$1 cm waveguide formed in a 230/20 torr Ar/N_2O gas mixture. Probe (70 ps, 532 nm) delay = 5 ns. (b) Phase map extracted from (a). The end curves represent the average phase along the section of waveguide shown.

be given to possible probe ray refraction by the plasma, since this would complicate interpretation of the interferogram. The maximum refraction would be expected near the top and bottom of the plasma, where the rays sample the highest transverse gradient regions. A ray trace using the density profiles extracted below indicates transverse displacements of less than $\sim\lambda/10$ at 532 nm. As another check, a 1064 nm probe was used under similar plasma conditions, and the extracted density profiles were very similar to those produced with the 532 nm probe. Since the angular deflection of 532 nm probe rays is 4 times smaller than for the 1064 nm probe, we concluded that refraction was negligible for our conditions.

A fast Fourier transform technique [14] was used to retrieve the plasma-imposed phase shift. This method allowed processing of the entire image at once, returning the phase shift as a function of both radial and axial positions. A plot of the phase shift obtained from Fig. 1(a) is shown in Fig. 1(b). Extraction of the electron density was then reduced to the Abel inversion problem for a radially symmetric object from which chordally integrated information (such as phase) is known [15]. Our phase maps were inverted along individual transverse phase lineouts (a vertical column of pixels down the image) or, in regions of axial uniformity, by first averaging many phase lineouts along the plasma axis. Averaging greatly reduces uncertainty from random fluctuations in the phase.

Figure 2 shows electron density plots obtained from the Abel inversion of raw phase data averaged over $\sim$200 lineouts for a background gas mixture of 230 torr Ar and 20 torr N_2O, with pump pulse energy of 500 mJ and peak intensity of 5×10^{13} W/cm^2. The gas N_2O has a relatively low breakdown threshold (with a spark appearing at intensities slightly below 10^{13} W/cm^2 for our 100 ps, 1064 nm pump pulses) and is used to provide seed electrons to assist collisional ionization of the dominant gas, here argon. The vertical bars on the $t = 180$ ps profile in Fig. 2(a) represent the statistical standard deviation of profiles derived from individual phase lineouts. At smaller radii the bars are larger due to fewer pixels contributing to the Abel inversion there. Uncertainty from calibration of the imaging system is less than 5%.

The data confirm the general features of channel formation predicted by our calculations and suggested by our guiding experiments. Figure 2(a) shows the electron density evolution up to 180 ps (the pump pulse peak occurs at $t = 0$). In this early range of delay, the interferograms are slightly blurred due to integration of the rapid dynamics over the 70 ps probe duration. The initial electron density is created in the line focus of the axicon and rapidly grows to a maximum on axis. This growth occurs during the laser pulse and continues for $\sim$100 ps past the peak, indicating that at this density, the contribution of heating and subsequent collisional ionization is important. The maximum on-axis electron density at early times ($<$200 ps), before expansion and shock development occur, can be used to obtain the peak average ionization level $\overline{Z}$ through $\overline{Z} \approx N_e/N_i$, where N_i corresponds to the original atom density in the gas target, obtained from the measured gas fill pressure. Since recombination occurs on a time scale of many nanoseconds [4], this average ionization level will be maintained for the full range of delays measured here. Figure 2(a) shows a peak density $N_e \approx 6 \times 10^{19}$ cm^{-3}, which gives a minimum of $\overline{Z}_{\text{argon}} \approx 7$ for the majority argon ions, assuming that at most the nitrogen and oxygen atoms are ionized to heliumlike states $\overline{Z}_{\text{nit}} \approx 5$ and $\overline{Z}_{\text{oxy}} \approx 6$. At higher fill pressures up to 330/20 torr of Ar/N_2O, we find $\overline{Z}_{\text{argon}}$ increases towards $\approx$8, in agreement with previous calculations [4]. By about 200 ps, the plasma has begun to expand into the background gas. The onset of shock development and the on-axis electron density minimum is seen in Fig. 2(b). Note that the density minimum develops well within 1 ns, consistent with earlier experiments showing the onset of leaky guiding around this delay, where the shock wall width and depth is still insufficient to confine the lowest order guided mode [5]. The sequence in Fig. 2(c) shows slowing of the expansion and flattening of the central density.

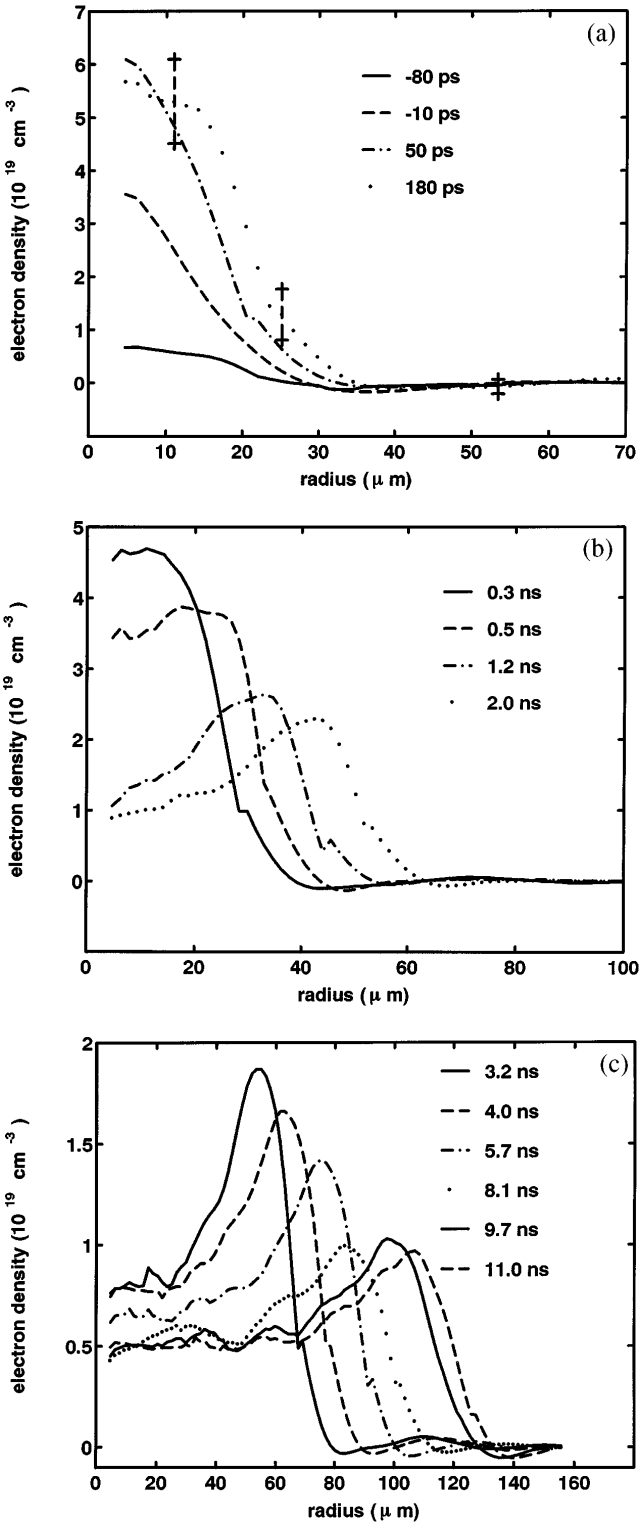

FIG. 2. Electron density profiles obtained from Abel inversion of raw phase data averaged over ~200 lineouts for 230/20 torr Ar/N_2O gas mixture. Vertical bars on the 180 ps data represent the standard deviation derived from individual phase lineouts.

The waveguide expansion for three different pressures (under the same peak pump intensity of 5×10^{13} W/cm^2) is shown in the shock position vs time plots of Fig. 3(a), with shock position taken as the half-maximum point in a phase plot. The data points are shown least squares fitted to the expression $R_s = \alpha t^m$, where the fits give $m = 0.51$ through 0.53 with maximum standard deviation 0.03, and the fit to α is a function of pressure. This is in good agreement with the expression for self-similar expansion of a cylindrical blast wave [16], $R(t) = \xi_0 (E_{\text{th}}/\rho_0)^{1/4} t^{1/2}$, where E_{th} is the thermal energy per unit length initially driving the expansion, ρ_0 is the initial mass density, and ξ_0 is a dimensionless parameter which is a function of the specific heat ratio and is of order unity. This expression applies to the phase of the expansion where hot "fluid" enclosed by the shock is cooling through expansion work. Using the fitted values of α for each pressure, and using $\xi_0 \approx 1$, gives $E_{\text{th}} = 3.5$, 4.9, and 6.2 mJ/cm for the 200, 250, and 300 torr cases. These are lower than would be expected from our measured pump absorption fractions of ~10%–15% in this range of pressure, indicating that rapid cooling has already taken place at earlier times, within a few hundred

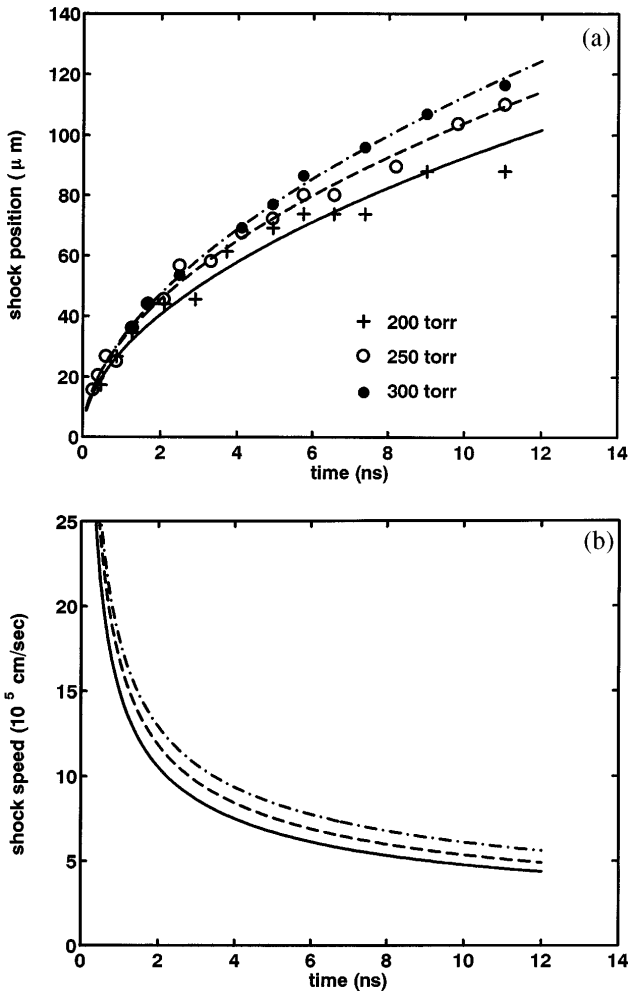

FIG. 3. (a) Shock position vs time for 180/20, 230/20, and 280/20 torr gas mixtures of Ar/N_2O. Least squares fits to $R_s = \alpha t^m$ are shown for each data set. Fits give $m = 0.51$ through 0.53 with a maximum standard deviation of 0.03. (b) The shock speed is calculated as the derivative of the fits in (a).

picoseconds of the pump pulse. Indeed, a code calculation for the 250 torr case and peak intensity 5×10^{13} W/cm^2 shows that the electron temperature reaches ~80 eV near the peak of the pump pulse and then rapidly cools to ~20 eV in the next 350 ps, with thermal conduction to the outer layer of ionizing gas dominating the temperature drop. Shock speed vs time [Fig. 3(b)] is calculated as the derivative of the curve fits to the data points of Fig. 3(a). A rapid decrease in the expansion rate is seen to occur in the first 2 nanoseconds. Since the pressure of the surrounding gas is negligible compared to the plasma pressure, the shock speed is related to the temperature T_e by $c_s \approx \sqrt{\gamma \bar{Z} k T_e / m_i}$, where γ is the ratio of specific heats and $\sqrt{\gamma}$ is of order unity. At $t \approx 400$ ps, using this expression with $c_s \approx 2 \times 10^6$ cm/sec (and $\bar{Z} \approx 7$) gives a profile average $T_e \sim 20$ eV, consistent with the code calculations mentioned above. By $t \approx 2$ ns, $T_e \sim 5$ eV. At longer times up to the maximum delay of 11 ns, the shock speed approaches 5×10^5 cm/sec, corresponding to a temperature of ~1 eV. The curve fits of Fig. 3(a) suggest that the temperature drop over the range of delay shown is attributable to expansion work, with other channels contributing weakly if at all. This is consistent with the estimated temperatures: for times beyond a few hundred picoseconds they are too low to cause significant extra collisional ionization at the plasma edge, which would have made conduction losses more important.

For coupling of intense pulses into plasma waveguides, the density profile at the waveguide entrance is of interest. As a visual aid, the profile displayed in Fig. 4 is reflected through its symmetry axis. The electron density minimum is seen to persist to within ~150 μm of the measurable end of the plasma. Within ~200 μm of the end, the fully developed density depression characteristic of the channel center region [Fig. 2(c)] is seen, with a slightly smaller radius. The overall density profile is generally uniform over the plasma length with tapering in the last few hundred microns. We will present the profiles for the evolution of full length channels in a longer paper.

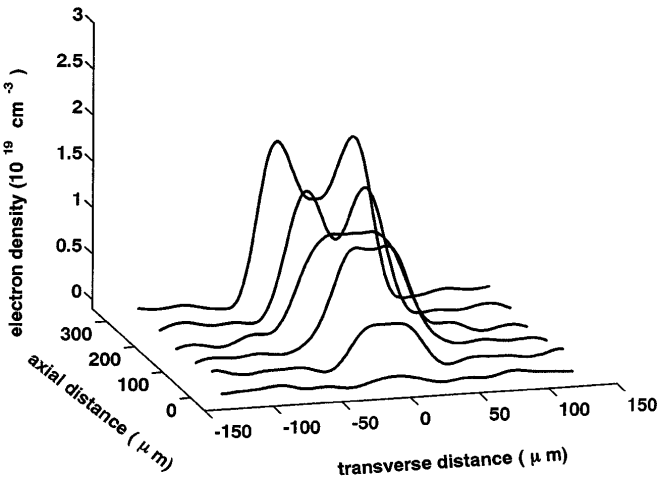

FIG. 4. End region of plasma waveguide produced in 200 torr N_2O at 4.7 ns delay, showing tapering of the electron density profile and the on-axis electron density depression persisting to within ~150 μm of the end.

The results presented here characterize and quantify many of the previously inferred aspects of the plasma waveguide. The shock development and channel formation begins on a ~100–200 ps time scale. The ionization level is enhanced with increased fill pressure. The waveguide plasma cools quite rapidly in the first few hundred picoseconds after generation, with expansion cooling dominating thereafter as the plasma expands as a cylindrical blast wave. Very long scale uniformity along the axis of the waveguide has also been demonstrated, and this is encouraging for applications requiring electron density control in guiding experiments.

This work is supported by the National Science Foundation (ECS-9224520 and PHY-9515509), the Air Force Office of Scientific Research (F49620-96-10095), and the National Institute of Standards and Technology (60NANB4D1648).

[1] H. M. Milchberg, T. R. Clark, C. G. Durfee, T. M. Antonsen, and P. Mora, Phys. Plasmas **3**, 2149 (1996).
[2] T. Tajima and J. M. Dawson, Phys. Rev. Lett. **43**, 267 (1979); P. Sprangle, E. Esarey, A. Ting, and G. Joyce, Appl. Phys. Lett. **53**, 2146 (1988).
[3] J. Krause, K. Schafer, and K. Kulander, Phys. Rev. Lett. **68**, 3535 (1992); C. G. Wahlstrom, S. Borgstrom, J. Larsson, and S. G. Pettersson, Phys. Rev. A **51**, 585 (1995).
[4] H. M. Milchberg, C. G. Durfee III, and J. Lynch, J. Opt. Soc. Am. B **12**, 731 (1995).
[5] C. G. Durfee III, J. Lynch, and H. M. Milchberg, Opt. Lett. **19**, 1937 (1994); P. Sprangle and E. Esarey, Phys. Fluids B **4**, 2241 (1992).
[6] H. M. Milchberg, C. G. Durfee III, and T. J. McIlrath, Phys. Rev. Lett. **75**, 2494 (1995).
[7] G. D. Zimmerman and W. L. Kruer, Comments Plasma Phys. Controlled Fusion **2**, 51 (1977).
[8] S. Jackel, S. Burris, J. Grun, A. Ting, C. Manka, K. Evans, and J. Kosakowskii, Opt. Lett. **20**, 1086 (1995).
[9] Y. Erlich, C. Cohen, A. Zigler, J. Krall, P. Sprangle, and E. Esarey, Phys. Rev. Lett. **77**, 4186 (1996).
[10] M. Dunne, T. Afshar-Rad, J. Edwards, A. J. MacKinnon, S. M. Viana, and O. Willi, Phys. Rev. Lett. **72**, 1024 (1994).
[11] P. E. Young, M. E. Foord, J. H. Hammer, W. L. Kruer, M. Tabak, and S. C. Wilks, Phys. Rev. Lett. **75**, 1082 (1995).
[12] C. G. Durfee III, T. R. Clark, and H. M. Milchberg, J. Opt. Soc. Am. B **13**, 59 (1996).
[13] J. A. Stamper, S. H. Gold, S. P. Obenschain, E. A. McLean, and L. Sica, J. Appl. Phys. **52**, 6562 (1981).
[14] M. Takeda, H. Ina, and S. Kobayashi, J. Opt. Soc. Am. B **72**, 156 (1981).
[15] I. H. Hutchinson, *Principles of Plasma Diagnostics* (Cambridge University Press, Cambridge, 1987).
[16] Y. A. Zeldovich and Y. P. Raizer, *Physics of Shock Waves and High-Temperature Hydrodynamic Phenomena* (Academic Press, New York, 1966).